SPC METHODS FOR DETECTING SIMPLE SAWING DEFECTS USING REAL-TIME LASER RANGE SENSOR DATA

*Christina Staudhammer**

Assistant Professor
School of Forest Resources and Conservation
University of Florida
349 Newins-Ziegler Hall
Gainesville, FL 32611-0410

Robert A. Kozak and *Thomas C. Maness*

Associate Professors
Faculty of Forestry
University of British Columbia
2424 Main Mall
Vancouver B.C. V6T 1Z4 Canada

(Received March 2005)

ABSTRACT

Effective statistical process control (SPC) procedures can greatly enhance product value and yield in the lumber industry, ensuring accuracy and minimum waste. To this end, many mills are implementing automated real-time SPC with non-contact laser range sensors (LRS). These systems have, thus far, had only limited success because of frequent false alarms and have led to tolerances being set excessively wide and real problems being missed. Current SPC algorithms are based on manual sampling methods and, consequently, are not appropriate for the volume of data generated by real-time systems. The objective of this research was to establish a system for real-time LRS size control data for automated lumber manufacturing. An SPC system was developed that incorporated multi-sensor data, and new SPC charts were developed that went beyond traditional size control methods, simultaneously monitoring multiple surfaces and specifically targeting common sawing defects. In this paper, eleven candidate control charts were evaluated. Traditional X-bar and range charts are suggested, which were explicitly developed to take into account the components of variance in the model. Applying these methods will lead to process improvements for sawmills using automated quality control systems, so that machines producing defective material can be identified and prompt repairs made.

Keywords: Lumber size control, statistical process control (SPC), control charts, real-time data collection, lumber manufacturing, simulation.

INTRODUCTION

For more than three decades, Shewhart control charts (Shewhart 1931) have helped automated lumber manufacturers to monitor the sawing process and produce lumber to consistent size standards. In order to successfully apply Shewhart's methods, process data must meet three assumptions: normality, independence, and homogeneity of variance (Mastrangelo et al. 2001). Under typical mill conditions, statistical process control (SPC) is conducted manually; a small group of sample boards is taken from the sawing process at infrequent time intervals and measured with digital calipers. Under these conditions, the three assumptions are met. The success of SPC programs has led to their widespread use in modern sawmills, and lumber manufacturers can directly attribute sizeable cost savings to their SPC practices (Maness 1993; Young and Winistorfer 1999).

New technologies for SPC in lumber manu-

* Corresponding author

facturing include laser range sensors (LRS), which make real-time measurement of the sawing process possible. When set up in-line with sawing machines, each piece of lumber processed is measured at a very fine scale, making thousands of measurements per sawn piece available. Moreover, these systems can be set up with multiple LRSs, enabling data collection on each side of each board. This is of particular interest in modern mills, where it is standard to cut the opposing sides of each board with different saws.

Many mills are now implementing real-time scanning technologies; however, SPC methods have not been updated to reflect the increased sampling frequency or the capacity of this new technology. Mills using LRSs have anecdotally reported that control limits must be set manually in order to prevent false out-of-control signals from overwhelming their systems. This is not surprising; current SPC methods do not transfer directly to this new real-time technology, as the statistical model which describes the real-time data is different from that of manual sampling. Moreover, SPC methods have not been updated to take advantage of the opportunity to better describe the sawing process with the additional data available.

Since real-time measurement systems take a very large number of autocorrelated observations on each side of each board, many of the assumptions needed to use the usual inferential statistics associated with SPC charts, e.g., independent and identically distributed (iid) data, are violated. Control charts must specifically take autocorrelation into account (Montgomery and Mastrangelo 1991), and where appropriate, alternative measures, such as control charts for dependent and/or non-normal data (Padgett and Spurrier 1990; Grimshaw and Alt 1997), need to be developed.

A statistical model describing real-time LRS measurements taken from multiple boards and multiple surfaces has been derived (Staudhammer et al. 2005). While the usual statistical model for SPC contains components for within- and between-board variation, the LRS model contains additional components of variance (COV) from laser positions and the interaction between boards and laser positions. These components provide the basis of a SPC system for monitoring measurable product attributes like average board size.

With the additional data made available by this technology, there is an opportunity to more thoroughly monitor the sawing process. Systems can be designed to target known causes of substandard product by identifying specific sawing defects. For example, Rasmussen et al. (2004) documented several sawing defects that are identifiable with laser scanning technology. Using multiple LRSs, an SPC system for real-time data has the capacity to better describe the sawing process and prevent production of lumber with specific kinds of defects. The objective of this paper is to present control charts based on a statistical model of the sequence of real-time LRS measurements. This system would be used to monitor the sawing process, targeting two specific kinds of defects common to automated sawmills, machine positioning defects and wedge.

BACKGROUND

Identifying simple sawing defects with SPC

Lumber shape defects occur frequently in the sawing process, and have a variety of causes. Fig. 1 shows a normal board versus two simple defects that are identifiable with laser scanning

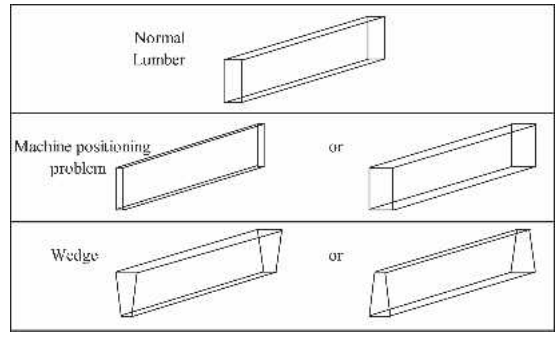

FIG. 1. Normal sawing versus two types of sawing defects.

technology (Rasmussen et al. 2004). Machine positioning or setworks problems occur when saw guides are not set to the correct distance, causing sawn boards to be too thick or too thin along the entire length of the board. This defect can occur because of software problems, worn parts, or improper pressure applied to saw guides (Maness et al. 2003). Whereas machine positioning problems tend to cause a uniform change across the width and length of the board, wedge is characterized by an unevenly sawn surface. Wedge often occurs when the saws are misaligned, causing a thickening (or thinning) from the bottom to the top of the board that is consistent along the length of the board (Rasmussen et al. 2004). These defects have obvious consequences for production mills, where products are made to meet specific customer tolerances.

With current methods, these defects are not always recognizable. As detailed in Maness et al. (2004), four charts are commonly used: the X-bar, R, S_w, and S_b charts (Table 1). When correct COV are used and groups of boards are sampled periodically, the X-bar and S charts have a false alarm rate of 0.27%, or an in-control average run length (ARL) of $1/0.0027 \approx 373$ (Montgomery 2001), and the R chart has a false

TABLE 1. *Commonly used SPC charts in lumber processing.*

Chart	Statistic Monitored	Control Limits
X-bar	Average board thickness	$CL = \overline{\overline{X}}$
		$LCL = \overline{\overline{X}} - 3\hat{\sigma}_{\overline{\overline{X}}}/c_4$
		$UCL = \overline{\overline{X}} + 3\hat{\sigma}_{\overline{\overline{X}}}/c_4$
R	Range of grouped board thickness averages	$CL = \overline{R}$
		$LCL = D_{0.001}\overline{R}/d_2$
		$UCL = D_{0.999}\overline{R}/d_2$
S_w	Within-board variability	$CL = \hat{\sigma}_w/c_4$
		$LCL = \left(\chi^2_{(0.0015;n-1)} \,/\, n-1\right)\hat{\sigma}_w/c_4$
		$UCL = \left(\chi^2_{(0.9985;n-1)} \,/\, n-1\right)\hat{\sigma}_w/c_4$
S_b	Between-board variability	$CL = \hat{\sigma}_b$
		$LCL = \hat{\sigma}_b\sqrt{\chi^2_{(0.0015;df)}/(df)}$
		$UCL = \hat{\sigma}_b\sqrt{\chi^2_{(0.9985;df)}/(df)}$

where: CL is the centreline;

LCL and UCL are the lower and upper control limits, respectively;

$\overline{\overline{X}}$ is the long-term estimate of the average thickness over all boards and measurement locations;

$\hat{\sigma}_{\overline{\overline{x}}} = \sqrt{\frac{\hat{\sigma}_b^2}{b} + \frac{\hat{\sigma}_w^2}{nb}}$;

$\hat{\sigma}_w^2$ and $\hat{\sigma}_b^2$ are long-term estimates of the within- and between-board variances, respectively;

c_4 and d_2 are control chart constants that correct for bias†;

$\overline{R}$ is the long term average range of board thickness values for groups of boards;

$D_{0.001}$ and $D_{0.999}$ are cumulative probability values for the range (Harter 1960);

$\chi^2_{(0.0015;n-1)}$ and $\chi^2_{(0.9985;n-1)}$ are cumulative probability values for chi-square distribution with n-1 degrees of freedom;

$df = \frac{(n\hat{\sigma}_b^2)^2}{\frac{MS_b^2}{b-1} + \frac{MS_w^2}{b(n-1)}}$; and

MS_b and MS_w are the between- and within-board mean squares from a one-way ANOVA

† For detailed derivation of these constants, see, for example, Montgomery (2001).

alarm rate of 0.2%, or an ARL of 1/0.002≈ 500.[1] If machine positioning problems result in consistent differences from the target, they are detected by a shift in the X-bar chart. If these problems are inconsistent, i.e., different from board to board, they are detected in a chart for between-board variation. Since data from each board are grouped together without regard to the location of the measurements along the board, wedge could easily be undetected by an X-bar chart. Although this defect would likely produce a signal on an S_w or R chart, so would other sawing defects, such as snake and taper.[2] It would then require further investigation on the part of SPC personnel to determine the exact cause of the chart's signal.

A model of real-time SPC data from laser range sensors

Commercially available real-time systems can be configured to scan both "face" sides of a board or cant as it leaves a sawing machine. Multiple LRSs can also be stacked so that multiple measurement streams are taken on each side of the board/cant. In such systems, multiple saws and saw types may be in use, giving rise to data from multiple sawing configurations. A mixed-effects model describing the real-time LRS measurements taken from multiple sawing configurations, boards, sides, and laser positions allowed for different variance components for each saw configuration × side combination (Staudhammer et al. 2005). The profile observations, y_{ijklm}, from the ith saw configuration (i = 1 to 4), jth side (j = 1 to 2), kth sample ($k = b_i$), lth laser location (l = 1 to 2), and mth distance along the board (m = 1 to n_{ijkl}) were modeled with random effects for boards (β_{ijk}), laser positions (λ_{ijl}), and their interaction ($\beta\lambda_{ijkl}$):

$$y_{ijklm} = \mu_{ij} + \beta_{ijk} + \lambda_{ijl} + \beta\lambda_{ijkl} + \varepsilon_{ijklm} \quad (1)$$

where: ε_{ijklm} = the residual error associated with the mth measurement from the lth laser location and kth sample board, in the ith saw configuration and jth side.

Within each saw configuration, residual plots showed model components were homoscedastic (i.e., $\mathrm{Var}(\varepsilon_{ijklm}) = \sigma_{\varepsilon_{ij}}^2$, $\mathrm{Var}(\beta_{ijk}) = \sigma_{\beta_{ij}}^2$, $\mathrm{Var}(\lambda_{ijl}) = \sigma_{\lambda_{ij}}^2$, and $\mathrm{Var}(\beta\lambda_{ijkl}) = \sigma_{\beta\lambda_{ij}}^2$). The sample board and board × laser position averages were found to be approximately normally distributed, with non-significant amounts of autocorrelation (Kolmogorov-Smirnov test, $\alpha > 0.25$), and this observation was further verified during field data collection using subsequently sawn boards. On the other hand, nearly every series of measurements taken from a single sample, side, and laser position exhibited large and significant amounts of autocorrelation for up to 200 lags for bandsawn and circular sawn boards and up to 50 lags for chipped boards (Fig. 2). In other words, bandsawn and circular sawn measurements separated by 200 observations showed high autocorrelation ($\rho > 0.5$). Further, a Kolmogorov-Smirnov test indicated that nearly every series of measurements taken from a single sample, side, and laser position was significantly non-normal ($\alpha = 0.05$). However, because autocorrelation results in inflated degrees

[1] In order to make direct comparisons to other charts with 3-Sigma limits, control limits that give a false alarm rate of ~0.27% are desired. This implies upper and lower quantiles of 0.0135% and 0.9865%; however, tabulated values for the distribution of ranges (Harter 1960) are only available at 0.001 increments, and thus, the closest values were used for this chart, as well as all other Range and Moving Range charts in this paper.

[2] Snake is a sawing defect in which an uneven wave pattern is present on the surface of the board, whereas taper is characterized by a gradual increase (or decrease) in thickness along the length of a board.

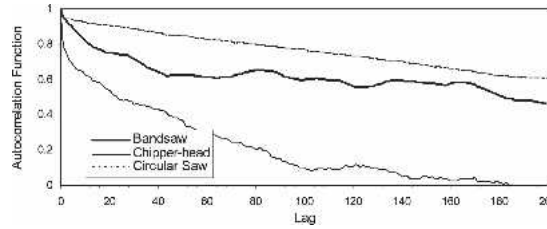

FIG. 2. Autocorrelation function for a single sample board × laser position series from each of three saw types.

of freedom, normality tests are excessively sensitive (Pardo-Iguzquiza and Dowd 2004).[3]

In order to describe individual observations taken by each LRS, the autocorrelation in the data needed to be explicitly accounted for. Using a multi-stage model, the autocorrelation in these errors were estimated in Staudhammer, et al. (2005) with autoregressive integrated moving average (ARIMA) models and ARIMA models modified for seasonal and long-memory effects (seasonal autoregressive fractionally integrated moving average, or SARFIMA models). The parameters from (1) were then fit with the estimated autocorrelated error covariance matrix.

This model provided a good description of the correlative structure within each sample board, side, and laser, and could be used with SPC methods developed exclusively for autocorrelated data (e.g., Montgomery and Mastrangelo 1991; Cook 1992; Gilbert et al. 1997; Lu and Reynolds 1999; Young and Winistorfer 2001; Noffsinger and Anderson 2002). In Young and Winistofer (2001), for example, the moisture content of medium-density fiberboard (MDF) samples taken at two to five-hour intervals were described by a first order autoregressive model (AR(1)). Residuals from this model were then plotted on SPC charts for individuals. Gilbert et al. (1997) collected subgrouped data from a container-filling process, and within these subgroups, measurements followed an AR(1) process. Shewhart control chart limits were instead adjusted to account for underestimation of the process variation caused by first order autocorrelation.

In the case of LRS data, the large autocorrelation is between subsequent measurements within each board. Using the techniques described above, an X-individuals chart could be applied to the stream of measurements, or subgroups could be formed by grouping measurements from each board. Although a rational subgroup should be chosen such that short-term within subgroup variation is captured, while allowing for variation to occur between subgroups (Gilbert et al. 1997), only a "logical" subgrouping may be possible without arbitrarily breaking the boards into sections or taking a sub-sample of measurements. If measurements taken from a single board constitute a subgroup, then model residuals could be charted using existing methods. However, given the ~3,000 measurements per board collected by the LRSs, the feasibility and utility of such an exercise are questionable. Moreover, Staudhammer, et al. (2005) found that if only summary statistics by sample and side are needed for SPC, the properties of the residual variance may not be as important. This is because autocorrelation does not affect the accuracy of averages, and the measure of the variation in these averages is a standard error that is comprised of components tied to each effect in the model. For example, the X-bar chart described by Maness et al. (2003) uses the standard error of the mean board thickness for a group of boards. Using the LRS model, this calculation uses the standard deviation of the mean by board and laser ($\bar{y}_{ijkl.}$), for each saw configuration and side (ij):

$$\sigma_{\bar{y}_{ijkl.}} = \sqrt{\operatorname{var}(\bar{\beta}_{ijkl.}) + \operatorname{var}(\bar{\lambda}_{ijkl.}) + \operatorname{var}(\overline{\beta\lambda}_{ijkl.}) + \operatorname{var}(\bar{\varepsilon}_{ijkl.})}$$

$$= \sqrt{\sigma^2_{\beta_{ij}} + \sigma^2_{\lambda_{ij}} + \sigma^2_{\beta\lambda_{ij}} + \operatorname{var}(\bar{\varepsilon}_{ijkl.})} \qquad (2)$$

In Staudhammer et al. (2005), it was shown that the variance of the average residuals ($\bar{\varepsilon}_{ijkl.}$) approaches zero when large numbers of observations are taken per board, side, and laser. Thus, the contribution of the residual variation ($\sigma_{\varepsilon_{ij}}{}^2$) to the standard error of the mean is negligible, and for use in detecting the common sawing defects described, the autocorrelation in the model can be ignored with only a negligible change in accuracy.

METHODS

Sample lumber data

In order to obtain multiple measurement stream data, a laboratory-based measurement

[3] This was confirmed by tests of sub-sampled data; in 100 random samples of 30 LRS measurements per board, side, and laser, only 14% showed significant departure from normality.

apparatus, which mimicked commercial systems, was set up in the Q-Lab of the Department of Wood Science in the Forest Sciences Centre at The University of British Columbia, Vancouver, Canada (Fig. 3). This apparatus consisted of a moving carriage, encoder, and four laser measurement devices. Four Hermary LRS-50 point laser range sensors were stack-mounted, two on each side of the carriage. Side 1-Laser 1 and Side 2-Laser 1 were vertically positioned to take measurements 2.54 cm (one in.) above the bottom of the board, Side 1-Laser 2 and Side 2-Laser 2 took measurements 2.54 cm (one in.) below the top of the board.

As the carriage moved the boards past the laser scanners at a controlled speed, the four streams of laser measurement data and encoder measurements of the location of the carriage were sent to a data concentrator and passed to a computer via Ethernet cable. The raw LRS data consisted of the distance from each of the four lasers to the wood surface, and the encoder data consisted of the distance along the length of the carriage. Under typical modern sawmill conditions, about 3,000 measurements can be taken with one LRS on an 8-foot board (Fig. 3).

Sample lumber obtained from Weyerhaeuser's New Westminster (British Columbia, Canada) sawmill consisted of 110 pieces of *Taruki*, a western hemlock (*Tsuga heterophyla*

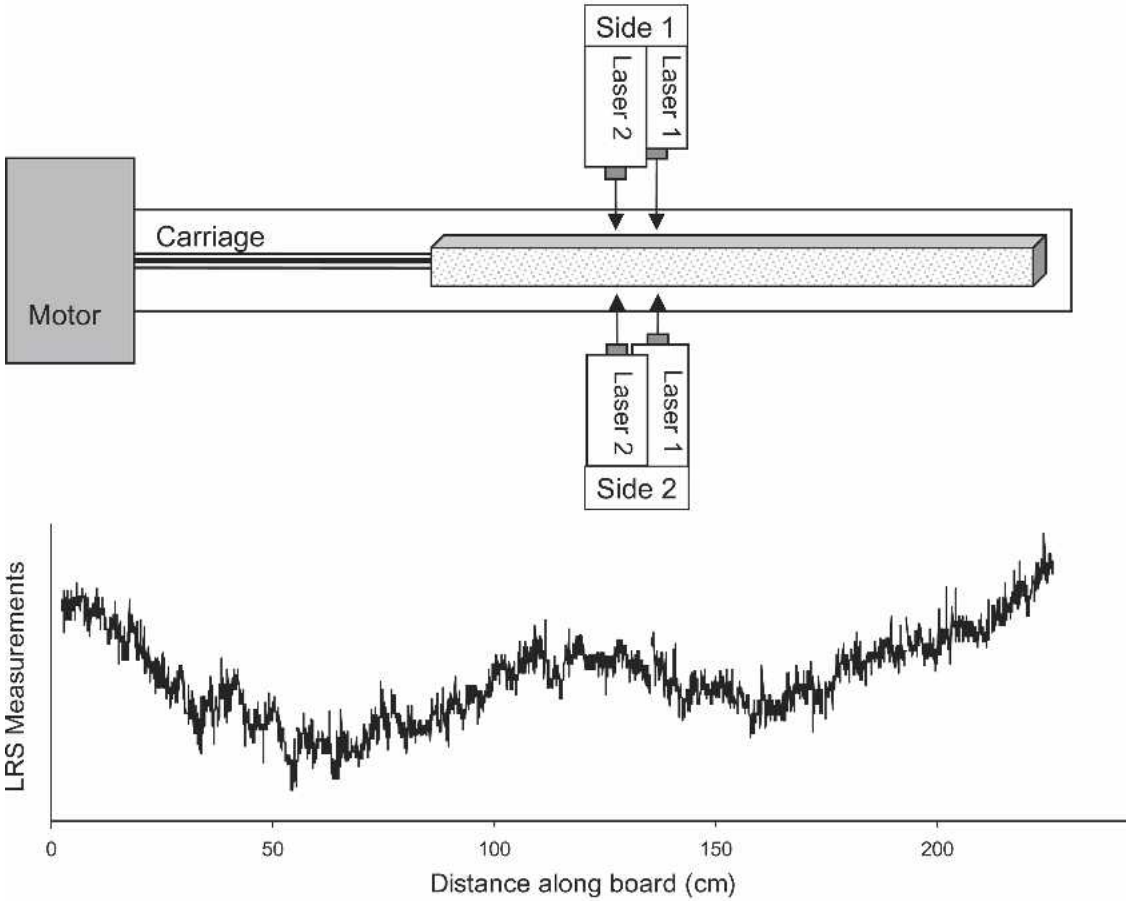

FIG. 3. Set up of LRS measurement apparatus (as viewed from above) and resulting LRS data from a single sample board, side, and laser position.

(Raf) Sarg.) dimension lumber product marketed to Japan with target thickness and width dimensions of 80 × 135 mm (2 1/32 × 5 5/16 in.), respectively. The green and un-planed samples of *Taruki* were removed from the mill processing line at the sorter. A random sample of lumber was desired to meet statistical assumptions. However, during normal mill operating conditions, only an arbitrary sample consisting of the first 100 pieces of *Taruki* sawn in a single shift was possible. On the other hand, since the mill was producing lumber of several species and dimensions, and there was substantial lag time between sawing and sorting, sampling did have a random element. These boards were considered a representative sample of lumber sawn during a period of hours.

The primary sawing of this lumber was done at the quad-bandsaw, and thus there were several cutting solutions with various saw configurations. Results were obtained separately for each of four saw configuration × side combinations: BB (both sides of the board bandsawn), BC (Side 1 bandsawn, Side 2 chipped), CB (Side 1 chipped, Side 2 bandsawn), and RR (both sides circular-sawn). Areas containing non-sawing defects, such as wane, were removed from these data manually, using the known positions of these defects mapped at the time of data collection. These data were then filtered for measurement errors using techniques from image processing (see Staudhammer 2004). Finally, these data were converted from distances (from the laser to the board surface) to profile quantities using the center of the board as a reference.

Proposed control charts

Control limits and other descriptors were developed to best detect the two common sawing defects using summary statistics within board. For each defect type, several candidate control charts are presented. The basis for these control charts are the average profile values by board and by laser, and the COV from the statistical model (1). When computing averages and COV, independent and identically distributed normal variates were assumed. Control limits were based on the traditional 3-sigma control charts originally developed by Shewhart (1931), and extended to processes exhibiting between- and within-part-size variability (Maness et al. 2003).

Control charts for lumber manufacturing have traditionally been based on subgrouping. Natural subgrouping occurred here because only small groups of boards were pulled periodically for SPC measurement. However, in real-time data collection, there is no obvious natural subgrouping, as the production of lumber is continuous with the exception of shift changes and breaks. To reflect this continuity, control charts for individuals were investigated where possible. On the other hand, subgrouping is necessary to construct control charts for the between-board variance ($\sigma_{\beta_{ij}}^2$). Control charts for moving statistics, such as the moving average and moving standard deviation, have been used in continuous processes; however, these charts tend to oversignal due to correlation introduced by using overlapping observations (Wheeler 1995). Therefore, artificial subgroups were created by taking groups of subsequent boards. In practice, subgroups could be formed based on time or by board location in a gang of multiple saws, for example.

Although multivariate charts have been suggested for use in industrial processes where multiple measurement streams are monitored (e.g., Young et al. 1999), they are most useful when a single chart does not provide enough information to decide if a process is in control (Wheeler 1995). Single multivariate charts have been found to be poor operationally, as out-of-control signals still must be investigated via univariate control charts in order to determine the cause of the signals (Does et al. 1999). That being the case, univariate control charts are suggested for each sawing defect type discussed as a part of a multi-chart SPC system for real-time size control; a single multivariate chart is not suggested. Rather, univariate charts targeting specific defects are proposed since they give more information than simple in-control/out-of-control signals in that each chart is related to a specific

TABLE 2. *Summary of proposed control charts.*

Defect Targeted	Name of Chart	Statistic monitored	Eq.
Machine positioning	X-bar$_{ind}$	Individual board averages: $\bar{y}_{i\cdot k\cdot\cdot}$	(3)
	X-bar$_{grp}$	Subgrouped board averages: $\bar{y}_{i\cdot g\cdot\cdot\cdot}$	(6)
	MR$_{\beta}$	Moving range of successive board averages: $MR(\bar{y}_{i\cdot k\cdot\cdot})_k$	(9)
	R$_{\beta_{grp}}$	Range of subgrouped board averages: $R(\bar{y}_{i\cdot gk\cdot\cdot})\|_{k=1}^{G}$	(11)
	S$_{\beta}$	Between board variation of subgrouped boards: $S^2_{\beta ijg}$	(13)
Wedge	R$_{\lambda_{ind}}$	Range of laser position averages within board by side: $R(\bar{y}_{ijkl\cdot})\|_{l=1}^{2}$	(16)
	R$_{\lambda_{grp}}$	Range of laser position averages within subgroup by side: $R(\bar{y}_{ijg\cdot l\cdot})\|_{l=1}^{2}$	(18)
	MR$_{\beta\lambda}$	Moving range of successive board averages by side and laser position: $MR(\bar{y}_{ijkl\cdot})_k$	(20)
	R$_{\beta\lambda_{grp}}$	Range of subgrouped board averages by side and laser position: $R(\bar{y}_{ijgkl\cdot})\|_{k=1}^{G}$	(22)
	S$_{\lambda}$	Between laser position variation for subgrouped boards by side: $S^2_{\lambda ijg}$	(24)
	S$_{\beta\lambda}$	Interaction of board × laser position variation for subgrouped boards by side: $S^2_{\beta\lambda ijg}$	(27)

sawing problem that can be addressed by mill staff.

The primary reason for choosing these types of charts is their ease of use and familiarity to mill personnel (Young and Winistorfer 1999), although more modern control charting techniques could have been investigated, such as the CUSUM and EWMA charts. Since these charts are often only recommended in conjunction with Shewhart charts (Woodall et al. 2000), they are not further investigated here. A summary of the proposed control charts is given in Table 2.

Proposed charts for machine positioning problems.—Because machine positioning problems are indicated when boards are consistently thicker or thinner along their entire lengths, monitoring for machine positioning problems was performed with control charts based on average board values. This included: (1) average profile by board, (2) range and moving range of subsequent board averages, and (3) between board variance.

X-bar$_{ind}$ Chart: An X-bar chart for individual boards (X-bar$_{ind}$ chart) was developed to monitor individual board averages, without using subgroups. An average profile was computed for each board ($\bar{y}_{i\cdot k\cdot\cdot}$), and these values were plotted on the X-bar$_{ind}$ chart. Control limits for a particular saw configuration (i) are given by:

$$\begin{aligned} CL &= T_i \\ LCL &= CL - 3\hat{\sigma}_{(\bar{y}_{i1k\cdot\cdot}+\bar{y}_{i2k\cdot\cdot})/2} \\ UCL &= CL + 3\hat{\sigma}_{(\bar{y}_{i1k\cdot\cdot}+\bar{y}_{i2k\cdot\cdot})/2} \end{aligned} \tag{3}$$

where: T_i is the target surface profile value; $\hat{\sigma}_{(\bar{y}_{i1k\cdot\cdot}+\bar{y}_{i2k\cdot\cdot})/2}$ is the estimated standard error of the average profile value by board for the ith sawing configuration; and $\bar{y}_{i1k\cdot\cdot}$ and $\bar{y}_{i2k\cdot\cdot}$ are the average Side 1 and Side 2 profiles values, respectively, for the ith saw configuration and kth board.

The target surface profile value is half the target thickness value for the sawing configuration. In this case, it was calculated as the long-term average of the two average profiles by side for the ith saw configuration ($\hat{\mu}_{i1\cdots}$ and $\hat{\mu}_{i2\cdots}$ from (1), respectively). These values were obtained from estimating the parameters of the mixed model in (1) with the SAS procedure PROC MIXED (Version 8.2, SAS Institute 2002).

Because y_{i1klm} and y_{i2klm} are independent, parameters in (1) are estimated by saw configuration and side. Thus, the standard errors in (3) were calculated using two sets of estimated model parameters:

$$\begin{aligned} \hat{\sigma}_{(\bar{y}_{i1k\cdot\cdot}+\bar{y}_{i2k\cdot\cdot})/2} &= \sqrt{\operatorname{var}\left(\frac{\bar{y}_{i1k\cdot\cdot}+\bar{y}_{i2k\cdot\cdot}}{2}\right)} \\ &= \sqrt{\frac{1}{4}\operatorname{var}(\bar{y}_{i1k\cdot\cdot}+\bar{y}_{i2k\cdot\cdot})} \\ &= \frac{1}{2}\sqrt{\hat{\sigma}^2_{\bar{y}_{i1k\cdot\cdot}}+\hat{\sigma}^2_{\bar{y}_{i2k\cdot\cdot}}} \end{aligned} \tag{4}$$

Using a components of variance approach with the number of laser positions per side = 2, (4) becomes:

$$\hat{\sigma}_{(\bar{y}_{i1k\cdot\cdot}+\bar{y}_{i2k\cdot\cdot})/2} = \frac{1}{2}\sqrt{\hat{\sigma}^2_{\beta_{i1}} + \frac{\hat{\sigma}^2_{\lambda_{i1}} + \hat{\sigma}^2_{\beta\lambda_{i1}}}{2} + \frac{\mathrm{var}(\bar{\varepsilon}_{i1kl\cdot})}{2} + \hat{\sigma}^2_{\beta_{i2}} + \frac{\hat{\sigma}^2_{\lambda_{i2}} + \hat{\sigma}^2_{\beta\lambda_{i2}}}{2} + \frac{\mathrm{var}(\bar{\varepsilon}_{i2kl\cdot})}{2}}$$

$$\cong \frac{1}{2}\sqrt{\hat{\sigma}^2_{\beta_{i1}} + \frac{\hat{\sigma}^2_{\lambda_{i1}} + \hat{\sigma}^2_{\beta\lambda_{i1}}}{2} + \hat{\sigma}^2_{\beta_{i2}} + \frac{\hat{\sigma}^2_{\lambda_{i2}} + \hat{\sigma}^2_{\beta\lambda_{i2}}}{2}} \quad (5)$$

where: $\hat{\sigma}^2_{\beta_{ij}}$, $\hat{\sigma}^2_{\lambda_{ij}}$, and $\hat{\sigma}^2_{\beta\lambda_{ij}}$ are estimates of the COV $\sigma^2_{\beta_{ij}}$, $\sigma^2_{\lambda_{ij}}$, and $\sigma^2_{\beta\lambda_{ij}}$, respectively, obtained from estimating the parameters of the mixed model in (1) with PROC MIXED.

X-bar$_{grp}$ Chart: Because sawing defects caused by machine positioning problems tend to occur in subsequently sawn boards, X-bar charts were also developed using groups of boards (X-bar$_{grp}$ chart). In manual SPC, natural subgroups occur as a consequence of periodic sampling. For these real-time data, artificial subgroups were created by taking successive groups of G boards. A range of subgrouping values was investigated, with G = 4, 6, 8, 10, 12, 16, and 20. Adding an additional subscript to denote the gth group of G boards, the group average profile for the ith saw configuration was $\bar{y}_{i\cdot g\cdot\cdot\cdot}$. These values were plotted on the X-bar$_{grp}$ chart with control limits for a particular saw configuration (i) given by:

$$\begin{aligned} CL &= T_i \\ LCL &= CL - 3\hat{\sigma}_{(\bar{y}_{i1g\cdot\cdot\cdot}+\bar{y}_{i2g\cdot\cdot\cdot})/2} \\ UCL &= CL + 3\hat{\sigma}_{(\bar{y}_{i1g\cdot\cdot\cdot}+\bar{y}_{i2g\cdot\cdot\cdot})/2} \end{aligned} \quad (6)$$

where: $\hat{\sigma}_{(\bar{y}_{i1g\cdot\cdot\cdot}+\bar{y}_{i2g\cdot\cdot\cdot})/2}$ is the estimated standard error of the average profile value by subgroup for the ith sawing configuration; and $\bar{y}_{i1g\cdot\cdot\cdot}$ and $\bar{y}_{i2g\cdot\cdot\cdot}$ are the average Side 1 and Side 2 profiles values, respectively, for the ith saw configuration, kth board, and gth group.

As in (3), the centerline is the target value, T_i, and the standard error term in (6) uses components from the models from each side. Using a components of variance approach and the estimated parameters from (1), the standard error for (6) was calculated as:

$$\hat{\sigma}_{(\bar{y}_{i1g\cdot\cdot\cdot}+\bar{y}_{i2g\cdot\cdot\cdot})/2} = 1/2\sqrt{\hat{\sigma}^2_{\bar{y}_{i1g\cdot\cdot\cdot}} + \hat{\sigma}^2_{\bar{y}_{i2g\cdot\cdot\cdot}}}$$

$$\cong \frac{1}{2}\sqrt{\frac{\hat{\sigma}^2_{\beta_{i1}} + \hat{\sigma}^2_{\beta_{i2}}}{G} + \frac{\hat{\sigma}^2_{\lambda_{i1}} + \hat{\sigma}^2_{\lambda_{i2}}}{2} + \frac{\hat{\sigma}^2_{\beta\lambda_{i1}} + \hat{\sigma}^2_{\beta\lambda_{i2}}}{2G}} \quad (7)$$

MR$_\beta$ Chart: The moving range (MR) is defined as the absolute difference between successive observations. Machine positioning problems are indicated by large differences between the average size of subsequently sawn boards, and thus, a moving range chart based on board averages (MR$_\beta$ chart) was constructed for detecting this sawing defect. For monitoring average profiles from individual boards, the moving range between the kth and (k + 1)th successive board averages in the ith saw configuration was computed as:

$$MR(\bar{y}_{i\cdot k\cdot\cdot})_k = |\bar{y}_{i\cdot,k,\cdot\cdot} - \bar{y}_{i\cdot,k+1,\cdot\cdot}| \quad (8)$$

These values were plotted on the MR$_\beta$ chart with control limits for a particular saw configuration (i) given by:

$$\begin{aligned} CL &= \overline{MR(\bar{y}_{i\cdot k\cdot\cdot})_{ki}} \\ LCL &= (D_{0.001}/d_2)\overline{MR(\bar{y}_{i\cdot k\cdot\cdot})_{k_i}} \\ UCL &= (D_{0.999}/d_2)\overline{MR(\bar{y}_{i\cdot k\cdot\cdot})_{k_i}} \end{aligned} \quad (9)$$

where: $\overline{MR(y_{i\cdot k\cdot\cdot})_{k_i}}$ is the average of the moving ranges between successive boards for the ith saw configuration.

R$_{\beta_{grp}}$ Chart: Machine positioning problems can also be found by examining the range of averages in a group of boards. Therefore, a range chart for subgrouped board averages (R$_{\beta_{grp}}$ chart) was constructed. Adding a subscript for groups, the board average in the gth subgroup and ith

saw configuration was $\bar{y}_{i\cdot gk\cdot\cdot}$. The range of these board averages was calculated as:

$$R(\bar{y}_{i\cdot gk\cdot\cdot})|_{k=1}^{G} = \text{Range}(\bar{y}_{i\cdot g1\cdot\cdot}, \bar{y}_{i\cdot g2\cdot\cdot}, \ldots, \bar{y}_{i\cdot gG\cdot\cdot}) \tag{10}$$

These values were plotted on the $R_{\beta_{grp}}$ chart with control limits for a particular saw configuration (i) given by:

$$\begin{aligned} CL &= \overline{R(\bar{y}_{i\cdot gk\cdot\cdot})|_{k=1}^{G}}_{i} \\ LCL &= \left(D_{0.001}/d_2\right)\overline{R(\bar{y}_{i\cdot gk\cdot\cdot})|_{k=1}^{G}}_{i} \\ UCL &= \left(D_{0.999}/d_2\right)\overline{R(\bar{y}_{i\cdot gk\cdot\cdot})|_{k=1}^{G}}_{i} \end{aligned} \tag{11}$$

where: $\overline{R(\bar{y}_{i\cdot gk\cdot\cdot})|_{k=1}^{G}}_{i}$ is the average of the $R(\bar{y}_{i\cdot gk\cdot\cdot})|_{k=1}^{G}$ values in the ith saw configuration.

S_β Chart: Machine positioning problems are indicated by an increase in the between-board variation. Thus, a control chart to monitor the variation due to boards was developed (S_β chart). Using artificial subgroups, the estimated between board variation for the ith saw configuration, jth side, and gth group ($S^2_{\beta_{ijg}}$) is a linear combination of the mean squares for board and board × laser in that group ($MS_{\beta_{ijg}}$ and $MS_{\beta\lambda_{ijg}}$, respectively):

$$S^2_{\beta_{ijg}} = \frac{MS_{\beta_{ijg}} - MS_{\beta\lambda_{ijg}}}{\sum_{l=1}^{2} \bar{n}_{ijg\cdot l}} \tag{12}$$

where: $\bar{n}_{ijg\cdot l}$ is the average number of observations per board in the gth group and lth laser position, for the ith saw configuration and jth side.

Values of $S^2_{\beta_{ijg}}$ were computed and plotted on the S_β chart. The control limits for a subgroup of size G in a particular saw configuration (i) and side (j) were calculated as:

$$\begin{aligned} CL &= \hat{\sigma}^2_{\beta_{ij}} \\ LCL &= \hat{\sigma}^2_{\beta_{ij}}\chi^2_{[1-\alpha/2;df]}/df(\beta_{ij})_G \\ UCL &= \hat{\sigma}^2_{\beta_{ij}}\chi^2_{[\alpha/2;df]}/df(\beta_{ij})_G \end{aligned} \tag{13}$$

where: $df(\beta_{ij})_G$ are the estimated degrees of freedom of the Chi-square distribution for $\sigma^2_{\beta_{ij}}$ in the ith saw configuration and jth side, with subgroup size G.

The degrees of freedom were approximated using the Satterthwaite procedure (Gaylor and Hopper 1969)[4]:

$$df(\beta_{ij})_G = \frac{(2\bar{n}_{ij\cdot\cdot}\hat{\sigma}^2_{\beta_{ij}})^2}{\frac{MS^2_{\beta_{ij}}}{G-1} + \frac{MS^2_{\beta\lambda_{ij}}}{G-1}} \tag{14}$$

where: $\bar{n}_{ij\cdot\cdot}$ is the average number of observations per board and laser position, for the ith saw configuration and jth side; and

$MS_{\beta_{ij}}$ and $MS_{\beta\lambda_{ij}}$ are the non-grouped mean squares underlying the estimated parameters from the mixed-effects model in (1).

Proposed charts for wedge.—Wedge is indicated by a difference between the top and the bottom laser position measurements (Fig. 1). Thus, monitoring for wedge involved comparing the profile values from the top versus bottom laser positions. This was accomplished with control charts for (1) ranges, and (2) the between-laser and board × laser interaction variances, $\sigma^2_{\lambda_{ij}}$ and $\sigma^2_{\beta\lambda_{ij}}$, respectively. Ranges were computed for average profile measurements between laser positions within board, and by board and laser position between subsequent boards.

$R_{\lambda_{ind}}$ Chart: To target the difference in average top and bottom profile measurements within board, an R chart for laser position averages within individual boards ($R_{\lambda_{ind}}$ chart) was developed. Since there are only two laser positions, the range between laser positions within each board for the ith saw configuration, jth side, and kth board was computed as:

$$R(\bar{y}_{ijkl\cdot})|_{l=1}^{2} = |\bar{y}_{ijk1\cdot} - \bar{y}_{ijk2\cdot}| \tag{15}$$

[4] In general, this approximation is appropriate when $MS_1/MS_2 > F_{(df1,\ df2;\ 0.9985)} * F_{(df2,\ df1;\ 0.5)}$, where MS_1 and MS_2 refer to the mean squares used in the df calculation (in this case, $MS_{\beta_{ij}}$ and $MS_{\beta\lambda_{ij}}$), and df_1 and df_2 refer to their respective degrees of freedom (Gaylor and Hopper 1969).

These values were plotted on the $R_{\lambda_{ind}}$ chart with control limits for a particular saw configuration (i) and side (j) given by:

$$\begin{aligned} CL &= \overline{R(\bar{y}_{ijkl\cdot})|^2_{l=1}}_{ij} \\ LCL &= (D_{0.001}/d_2)\overline{R(\bar{y}_{ijkl\cdot})|^2_{l=1}}_{ij} \\ UCL &= (D_{0.999}/d_2)\overline{R(\bar{y}_{ijkl\cdot})|^2_{l=1}}_{ij} \end{aligned} \quad (16)$$

where: $\overline{R(\bar{y}_{ijkl\cdot})|^2_{l=1}}_{ij}$ is the average of $R(\bar{y}_{ijkl\cdot})|^2_{l=1}$ values for the ith saw configuration and jth side.

$R_{\lambda_{grp}}$ Chart: In the presence of wedge, subsequent groups of boards will exhibit differences between the average profile computed for the top and bottom laser positions, and thus a range chart was developed to monitor laser position averages using artificial subgroups ($R_{\lambda_{grp}}$ chart). Adding a subscript to denote the gth subgroup formed from G successive sample boards, the average profile by group and laser position for the ith saw configuration and jth side is $\bar{y}_{ijg\cdot l\cdot}$. Since there are only two laser positions, the range of these average profile values was calculated for each group as:

$$R(\bar{y}_{ijg\cdot l\cdot})|^2_{l=1} = |\bar{y}_{ijg\cdot 1\cdot} - \bar{y}_{ijg\cdot 2\cdot}| \quad (17)$$

These values were plotted on the $R_{\lambda_{grp}}$ chart with control limits for a particular saw configuration (i) and side (j) given by:

$$\begin{aligned} CL &= \overline{R(\bar{y}_{ijg\cdot l\cdot})|^2_{l=1}}_{ij} \\ LCL &= (D_{0.001}/d_2)\overline{R(\bar{y}_{ijg\cdot l\cdot})|^2_{l=1}}_{ij} \\ UCL &= (D_{0.999}/d_2)\overline{R(\bar{y}_{ijg\cdot l\cdot})|^2_{l=1}}_{ij} \end{aligned} \quad (18)$$

where: $\overline{R(\bar{y}_{ijg\cdot l\cdot})|^2_{l=1}}_{ij}$ is the average of $R(\bar{y}_{ijg\cdot l\cdot})|^2_{l=1}$ values for the ith saw configuration, jth side.

$MR_{\beta\lambda}$ Chart: Wedge is also indicated by a change in the average values of subsequent profile measurements by board and laser position. Thus, a moving range chart was developed for the average profile values by board and laser position ($MR_{\beta\lambda}$ chart). Using individual board values, a moving range between subsequent boards for the ith saw configuration and jth side was computed for each lth laser position as:

$$MR(\bar{y}_{ijkl\cdot})_k = |\bar{y}_{ij,k,l\cdot} - \bar{y}_{ij,k+1,l\cdot}| \quad (19)$$

These values were plotted on the $MR_{\beta\lambda}$ chart with control limits for a particular saw configuration (i), side (j), and laser position (l) given by:

$$\begin{aligned} CL &= \overline{MR(\bar{y}_{ijkl\cdot})_{k}}_{ijl} \\ LCL &= (D_{0.001}/d_2)\overline{MR(\bar{y}_{ijkl\cdot})_{k}}_{ijl} \\ UCL &= (D_{0.999}/d_2)\overline{MR(\bar{y}_{ijkl\cdot})_{k}}_{ijl} \end{aligned} \quad (20)$$

where: $\overline{MR(\bar{y}_{ijkl\cdot})_{k}}_{ijl}$ is the average of all $MR(\bar{y}_{ijkl\cdot})_k$ values for the ith saw configuration, jth side, and lth laser position.

$R_{\beta\lambda_{grp}}$ Chart: The change in average profile measurements by board and laser position was also be monitored by group. Range charts were constructed for subgroups of board by laser averages ($R_{\beta\lambda_{grp}}$ chart). Adding a subscript for the gth subgroup, the average profile was computed for each board × laser within each subgroup: $\bar{y}_{ijgkl\cdot}$. The range of these averages within each subgroup for the ith saw configuration, jth side, and lth laser position was calculated as:

$$R(\bar{y}_{ijgkl\cdot})|^G_{k=1} = \text{Range}(\bar{y}_{ijg1l\cdot}, \bar{y}_{ijg2l\cdot}, \ldots, \bar{y}_{ijgGl\cdot}) \quad (21)$$

These values were plotted on the $R_{\beta\lambda_{grp}}$ chart with control limits for a particular saw configuration (i), side (j), and laser position (l) given by:

$$\begin{aligned} CL &= \overline{R(\bar{y}_{ijgkl\cdot})|^G_{k=1}}_{ijl} \\ LCL &= (D_{0.001}/d_2)\overline{R(\bar{y}_{ijgkl\cdot})|^G_{k=1}}_{ijl} \\ UCL &= (D_{0.999}/d_2)\overline{R(\bar{y}_{ijgkl\cdot})|^G_{k=1}}_{ijl} \end{aligned} \quad (22)$$

where: $\overline{R(\bar{y}_{ijgkl\cdot})|^G_{k=1}}_{ijl}$ is the average of the $R(\bar{y}_{ijgkl\cdot})|^G_{k=1}$ values in the ith saw configuration, jth side, and lth laser position.

S_λ Chart: Wedge results in high laser-to-laser variation. Thus, a chart was developed to monitor the between laser variation (S_λ chart). For the ith saw configuration, jth side, and gth group, the between laser variation ($S^2_{\lambda ijg}$) is a linear combination of the mean squares for laser and

laser × board in that group ($MS_{\lambda_{ijg}}$ and $MS_{\beta\lambda_{ijg}}$, respectively):

$$S^2_{\lambda_{ijg}} = \frac{MS_{\lambda_{ijg}} - MS_{\beta\lambda_{ijg}}}{\sum_{k=1}^{G} \bar{n}_{ijgk\cdot}} \tag{23}$$

where: $\bar{n}_{ijgk\cdot}$ is the average number of observations per laser in the *g*th group and *k*th board, for the *i*th saw configuration and *j*th side.

Values of $S^2_{\lambda ijg}$ were computed and plotted on the S_λ chart, with control limits for subgroup size *G* in a particular saw configuration (*i*) and side (*j*) calculated as:

$$\begin{aligned} CL &= \hat{\sigma}^2_{\lambda_{ij}} \\ LCL &= \hat{\sigma}^2_{\lambda_{ij}} \chi^2_{[1-\alpha/2;df]}/df(\lambda_{ij})_G \\ UCL &= \hat{\sigma}^2_{\lambda_{ij}} \chi^2_{[\alpha/2;df]}/df(\lambda_{ij})_G \end{aligned} \tag{24}$$

where: $df(\lambda_{ij})_G$ are the estimated degrees of freedom of the Chi-square distribution for $\sigma^2_{\lambda ij}$ in the *i*th saw configuration, and *j*th side, with subgroup size *G*.

The degrees of freedom were approximated with the Satterthwaite procedure as in Eq. (14), using the mean squares and degrees of freedom associated with calculating $S^2_{\lambda ijg}$:

$$\begin{aligned} df(\lambda_{ij})_G = (G\bar{n}_{ij\cdot\cdot}\hat{\sigma}^2_{\lambda_{ij}})^2/(MS^2_{\lambda_{ij}}/1 \\ + MS^2_{\beta\lambda_{ij}}/(G-1)) \end{aligned} \tag{25}$$

where: $MS_{\lambda_{ij}}$ and $MS_{\beta\lambda_{ij}}$ are the non-grouped mean squares underlying the estimated parameters from the mixed-effects model in (1).

$S_{\beta\lambda}$ Chart: Because wedge can result in high interaction variation of boards and laser positions, the $S_{\beta\lambda}$ chart was developed. The board × laser position variance for the *i*th saw configuration, *j*th side, and *g*th group ($S^2_{\beta\lambda_{ijg}}$) is a linear combination of the mean squares for board × laser and mean squares residual for that group ($MS_{\beta\lambda_{ijg}}$ and $MS_{\varepsilon_{ijg}}$, respectively):

$$S^2_{\beta\lambda_{ijg}} = \frac{MS_{\beta\lambda_{ijg}} - MS_{\varepsilon ijg}}{\bar{n}_{ijg\cdot\cdot}} \tag{26}$$

where: $\bar{n}_{ijg\cdots}$ is the average number of observations per board and laser position in the *g*th group, for the *i*th saw configuration and *j*th side.

Values of $S^2_{\beta\lambda_{ijg}}$ were computed and plotted on the $S_{\beta\lambda}$ chart. The control limits for a subgroup of size *G* in a particular saw configuration (*i*) and side (*j*) were calculated as:

$$\begin{aligned} CL &= \hat{\sigma}^2_{\beta\lambda_{ij}} \\ LCL &= \hat{\sigma}^2_{\beta\lambda_{ij}} \chi^2_{[1-\alpha/2;df]}/df(\beta\lambda_{ij})_G \\ UCL &= \hat{\sigma}^2_{\beta\lambda_{ij}} \chi^2_{[\alpha/2;df]}/df(\beta\lambda_{ij})_G \end{aligned} \tag{27}$$

where: $df(\beta\lambda_{ij})_G$ are the estimated degrees of freedom of the Chi-square distribution for $\sigma^2_{\beta\lambda_{ij}}$ in the *i*th saw configuration and *j*th side, with subgroup size *G*.

The degrees of freedom were approximated as in Eqs. (14) and (25):

$$\begin{aligned} df(\beta\lambda_{ij})_G = (\bar{n}_{ij\cdot\cdot}\hat{\sigma}^2_{\beta\lambda_{ij}})^2/(MS^2_{\beta\lambda_{ij}}/(G-1) \\ + MS^2_{\varepsilon ij}/(2G(\bar{n}_{ij\cdot\cdot}-1))) \end{aligned} \tag{28}$$

where: $MS_{\beta\lambda_{ij}}$ and $MS_{\varepsilon_{ij}}$ are the non-grouped mean squares underlying the estimated parameters from the mixed-effects model in (1).

Evaluation of proposed charts

Ideally, a new SPC system should be evaluated in the field under operational mill conditions. However, it was not possible for the mill to accommodate our data collection design and research schedule. Instead, Monte Carlo simulation methods were applied. Using the lab scan data, the SAS procedure PROC MIXED gave estimates of all mixed-effects and components of variance from the model in Eq. (1). These parameter estimates were used to simulate LRS data arising from (1), as well as to construct control limits. The Monte Carlo simulation was used to evaluate the performance of the charts under both in-control and out-of-control conditions. Average profiles by board, side, and laser position were simulated for each saw configuration and side using the following steps:

TABLE 3. *Investigated ranges of defect severities.*

Defect	Parameter	Range (mm)†	Range (inches) †
Machine positioning	Δ_m	±0.25, 0.50, 0.75, 1.00	±0.010, 0.020, 0.030, 0.040
Wedge	Δ_w	±0.25, 0.50, 0.75, 1.00	±0.010, 0.020, 0.030, 0.040

† This amount is added to both sides of the board, making the effective change in board thickness two times the range.

For each simulated board, a random board effect was generated: $B_{ijk} \sim N(0,\hat{\sigma}^2_{\beta_{ij}})$;

For each simulated laser position, a random laser position effect was generated: $L_{ijl} \sim N(0,\hat{\sigma}^2_{\lambda_{ij}})$;

For each simulated board and laser position, a random board × laser effect was generated: $BL_{ijkl} \sim N(0,\hat{\sigma}^2_{\beta\lambda_{ij}})$; and

Using the estimate of the overall average profile value by saw configuration and side ($\hat{\mu}_{ij}$), the simulated average profile by board × side × laser position was calculated as:

$$\tilde{\bar{y}}_{ijkl} = \hat{\mu}_{ij} + B_{ijk} + L_{ijl} + BL_{ijkl}$$

Simulated data were created for various subgrouping scenarios. One thousand sample groups were created, with 1, 4, 6, 8, 10, 12, 16, and 20 boards per group. To generate simulated profile observations within each group, board, side, and laser position, simulated autocorrelated errors (e_{ijklm}) were added to the simulated profile averages (from Step 4):

$$\tilde{y}_{ijklm} = \tilde{\bar{y}}_{ijkl} + e_{ijklm}$$

These autocorrelated errors were generated using the ARIMA and seasonal ARIMA models, as detailed in Staudhammer et al. (2005).

For evaluating the ability of the charts to detect specific sawing defects, out-of-control data were generated by modifying the simulated data to include each type of defect using graduated levels of severity. To generate boards with machine positioning problems and wedge, the simulated profile observations were modified uniformly along the length of the board. For machine positioning problems, this was accomplished by adding an amount, Δ_m, to each board, side, and laser position observation. For wedge, an amount, $\Delta_w/2$, was added to the top laser position observations, while the same amount, $\Delta_w/2$, was subtracted from the bottom laser position observations. The values of Δ_m and Δ_w were chosen to represent a range of defect severities, from small to severe. These values were chosen in consultation with industry sawing experts (G.S. Shajer and D.C. Wong[5], personal communication, 2004), and are shown in Table 3.

The proposed charts were evaluated using the simulated in-control and out-of-control data. For in-control data, the false alarm rate was evaluated. For out-of-control data, the rate of chart signaling was evaluated. To evaluate out-of-control performance of the five charts proposed for machine positioning problems and six charts proposed for wedge, all eleven charts were subjected to both machine positioning defect deviations and wedge defect deviations. This provided a wide variety of testing conditions and allowed testing of chart by defect interactions.

RESULTS

Proposed charts for machine positioning problems

The in-control performance of the X-bar charts for individuals (X-bar$_{ind}$, Eq. (3)) and groups (X-bar$_{grp}$, Eq. (6)) is shown in Fig. 4(a) by saw configuration, with $G = 1$ corresponding to X-bar$_{ind}$. The expected proportion of out-of-control signals is shown as a reference line drawn at 0.27%, which corresponds to the ARL of 3-sigma control charts under the assumption of normality. While the number of out-of-control signals by subgroup size varied, the overall average was on target at 0.3%, and there was no consistent trend or pattern by saw configuration or subgroup size.

[5] Professor, Department of Mechanical Engineering, The University of British Columbia, and Wood Machining Scientist, Forintek Canada Corporation, respectively (Vancouver, B.C. Canada).

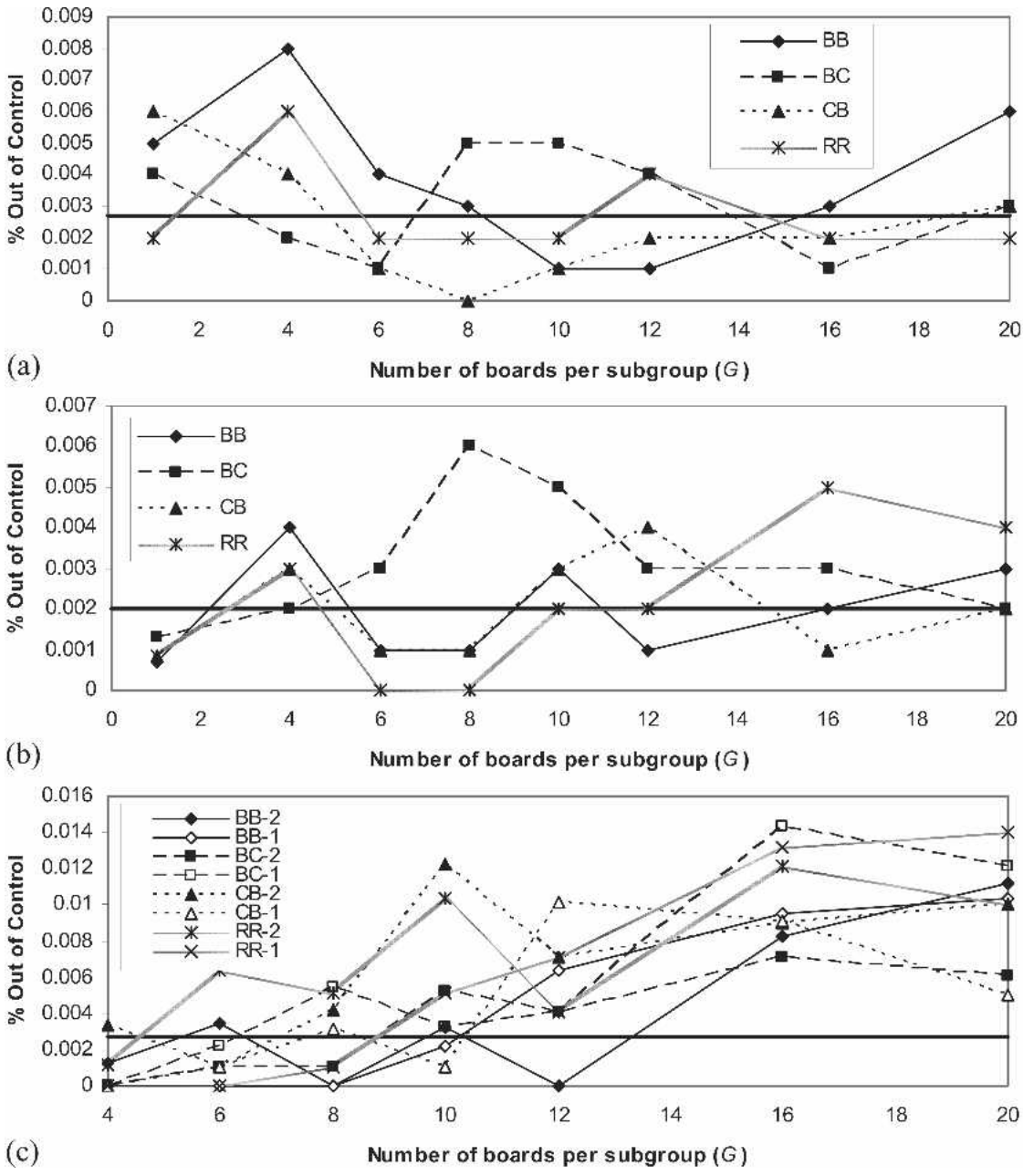

FIG. 4. Percent out of control for (a) X-bar$_{ind}$ (G = 1) and X-bar$_{grp}$ charts, (b) MR$_{\beta}$ (G = 1) and R$_{\beta_{grp}}$ charts, and (c) S$_{\beta}$ chart, by subgroup size (G) and saw configuration[6].

[6] The following abbreviations are used in figures throughout the remainder of this paper: BB = Bandsaw-Bandsaw Saw Configuration, BC = Bandsaw-Chipper-head Saw Configuration, CB = Chipper-head-Bandsaw Saw Configuration, RR = Circular saw-Circular Saw Configuration, BB-1 = Side 1 of BB Saw Configuration, BB-2 = Side 2 of BB Saw Configuration, etc.

The in-control results for the MR_{β} and $R_{\beta_{grp}}$ charts (Eqs. (9) and (11), respectively) are shown in Fig. 4(b) (with $G = 1$ corresponding to the moving range chart). The expected number of out-of-control signals is shown as a reference line at 0.2%, which corresponds to the ARL of the closest values available for the cumulative range distribution (Harter 1960). On average, the number of simulated out-of-controls was 0.25%. There was no obvious consistent trend by number of boards per subgroup or saw configuration.

Results for the S_{β} chart (Eq. (13)) using in-control simulations are shown in Fig. 4(c). This chart was affected by group size, performing best with moderate group sizes. At most group sizes, the number of out-of-control signals was well above the reference line for the expected number of out-of-controls (0.27%). This behavior was likely a result of the Satterthwaite procedure being applied outside of its recommended range.

"Power curves" for the X-bar_{ind} and X-bar_{grp} charts for simulated BB boards are shown in Fig. 5(a) by subgroup size (with X-bar_{ind} shown as $G = 1$). These curves show the power of the chart to detect machine positioning deviations over various values of Δ_m. Since the response of the chart to negative and positive values of Δ_m was almost identical, only positive values are shown. It is not surprising that the chart with the largest subgroup size had more out-of-control signals at a smaller level of deviation, since this chart was

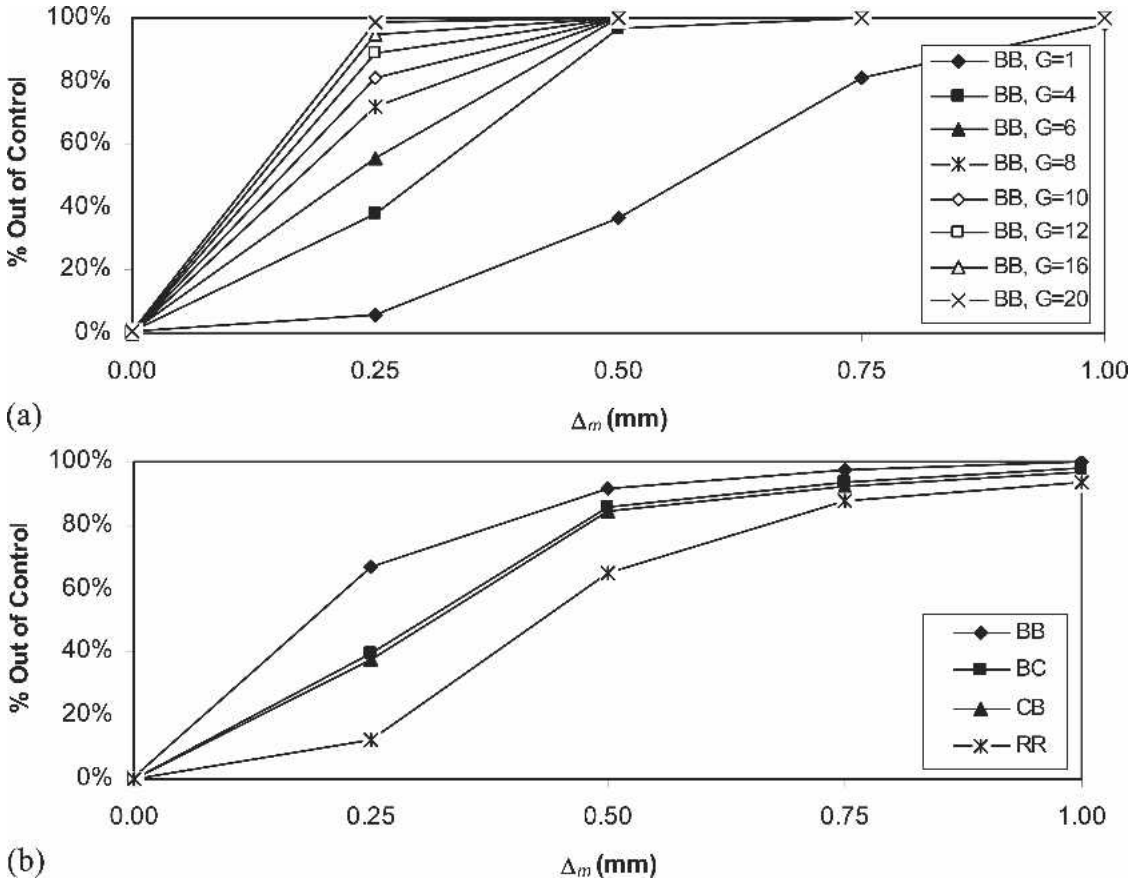

FIG. 5. Percent out of control size of simulated machine positioning deviation (Δ_m) for X-bar_{ind} ($G = 1$) and X-bar_{grp} charts by (a) subgroup size (G) for Saw Configuration BB, and (b) saw configuration and side (average of all subgroups is shown).

updated with information from twenty boards at a time. The behavior of this chart was similar for each type of saw configuration (Fig. 5(b)), except at smaller deviations, where saw configuration RR was slower to respond.

With the introduction of machine positioning deviations, the only indication in the MR_{β} and $R_{\beta_{grp}}$ charts was a single out-of-control signal the first time the deviation was introduced. Moreover, the machine positioning change was missed by the $R_{\beta_{grp}}$ chart entirely unless the deviation was introduced mid-subgroup. The S_{β} chart responded similarly; a single out-of-control was signaled at the first group with machine positioning problems only if the deviation was introduced in the middle of the subgroup. As in the X-bar charts, charts with larger subgroups were more likely to signal, as their control limits were narrower; however, only one signal was recorded. These charts produced flat power curves and are, therefore, not shown.

Proposed charts for wedge

The in-control performance of the $R_{\lambda_{ind}}$ and $R_{\lambda_{grp}}$ charts (Eqs. (16) and (18)) are shown in Fig. 6(a) (with $R_{\lambda_{ind}}$ shown as $G = 1$). The number of out-of-control signals for the $R_{\lambda_{ind}}$ and $R_{\lambda_{grp}}$ charts averaged 0.1%, slightly lower than the reference line at the expected value of 0.2%. The rate of out-of-controls was stable, with no obvious trend by number of boards per subgroup or saw configuration.

The results of in-control simulations for the $MR_{\beta\lambda}$ and $R_{\beta\lambda_{grp}}$ charts (Eqs. (20) and (22)) are shown in Fig. 6(b) by saw configuration and side, with $MR_{\beta\lambda}$ shown as $G = 1$. $MR_{\beta\lambda}$ and $R_{\beta\lambda_{grp}}$ charts were produced for each laser position; however, since their performance was nearly identical by laser, the average performance is shown. On average, the number of out-of-controls was on target with the expected value, shown as a reference line at 0.2%. Like the previous chart, there was no obvious trend by number of boards per subgroup or saw configuration.

The in-control S_{λ} chart for between-laser variation and $S_{\beta\lambda}$ chart for board × laser interaction variation (Eqs. (24) and (27), respectively) are shown in Fig. 6(c) and (d), respectively. The S_{λ} chart was greatly affected by subgroup sizes; it performed very poorly for small subgroups, but improved with larger subgroups. This improvement was due to increased degrees of freedom associated with larger subgroup sizes. The $S_{\beta\lambda}$ chart was more stable; the numbers of out-of-control signals were more in line with the expected values, at 0.2% on average.

Power curves constructed for the $R_{\lambda_{ind}}$ and $R_{\lambda_{grp}}$ charts are shown in Fig. 7(a). These charts responded with more out of controls as the size of the wedge deviation and subgroup size increased (Fig. 7(a-i)). Because there was a similar pattern for all saw configurations, the results of introducing wedge deviations are shown by subgroup for the BB saw configuration, Side 2 only. As in the X-bar chart with Δ_m, results for negative and positive values of Δ_w were very similar, and thus only positive values are shown. As expected, larger deviations in Δ_w produced more out-of-control signals. The average response over all subgroup sizes is shown to emphasize the different responses by saw configuration (Fig. 7(a-ii)); BB saw configurations were more responsive to increases in Δ_w, while RR saw configurations were less responsive.

The results of introducing a wedge deviation to the S_{λ} chart are shown in Fig. 7(b) by deviation size (Δ_w). As shown for in Fig. 7(b-i) with saw configuration RR, Side 1, these charts varied less by subgroup size. As in the previous charts, results for negative values of Δ_w were similar to those of the positive values, and thus only positive values are shown. The results for the S_{λ} chart by subgroup were similar within saw configuration and side, and minimal in comparison to the effect of Δ_w. Thus, results averaged over all subgroups are shown in Fig. 7(b-ii) by saw configuration and side. As expected, larger deviations in Δ_w produced more out-of-control signals. As in the range charts above, the results for the RR saw configurations were less responsive to the size of Δ_w than those of the other saw configurations.

The introduction of wedge deviations did not affect the performance of the $S_{\beta\lambda}$, $MR_{\beta\lambda}$, or

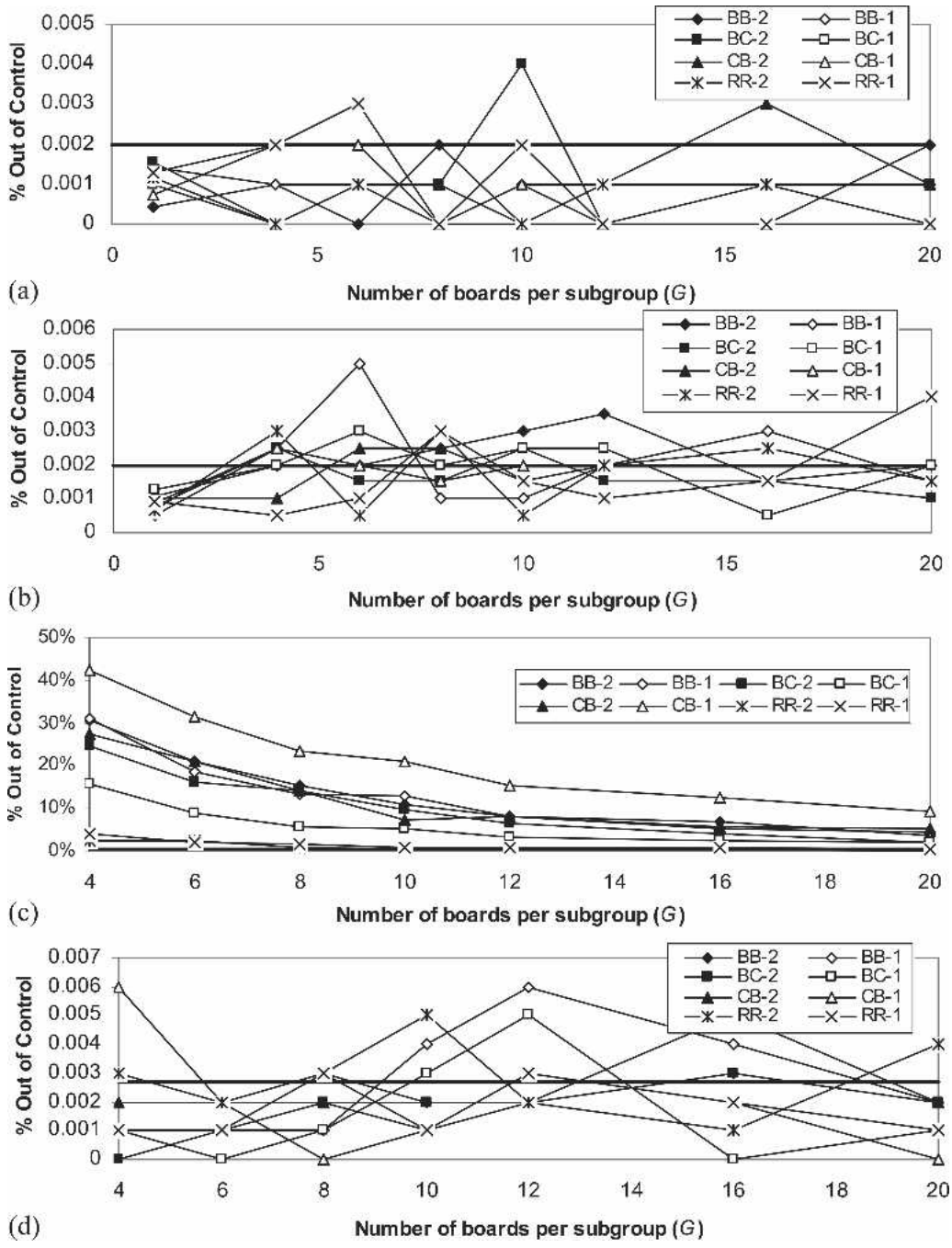

FIG. 6. Percent out-of-control by subgroup size (G), saw configuration, and side for (a) $R_{\lambda_{ind}}$ (G = 1) and $R_{\lambda_{grp}}$ charts, (b) $MR_{\beta\lambda}$ (G = 1) and $R_{\beta\lambda_{grp}}$ charts, (c) S_{λ} chart, and (d) $S_{\beta\lambda}$ chart.

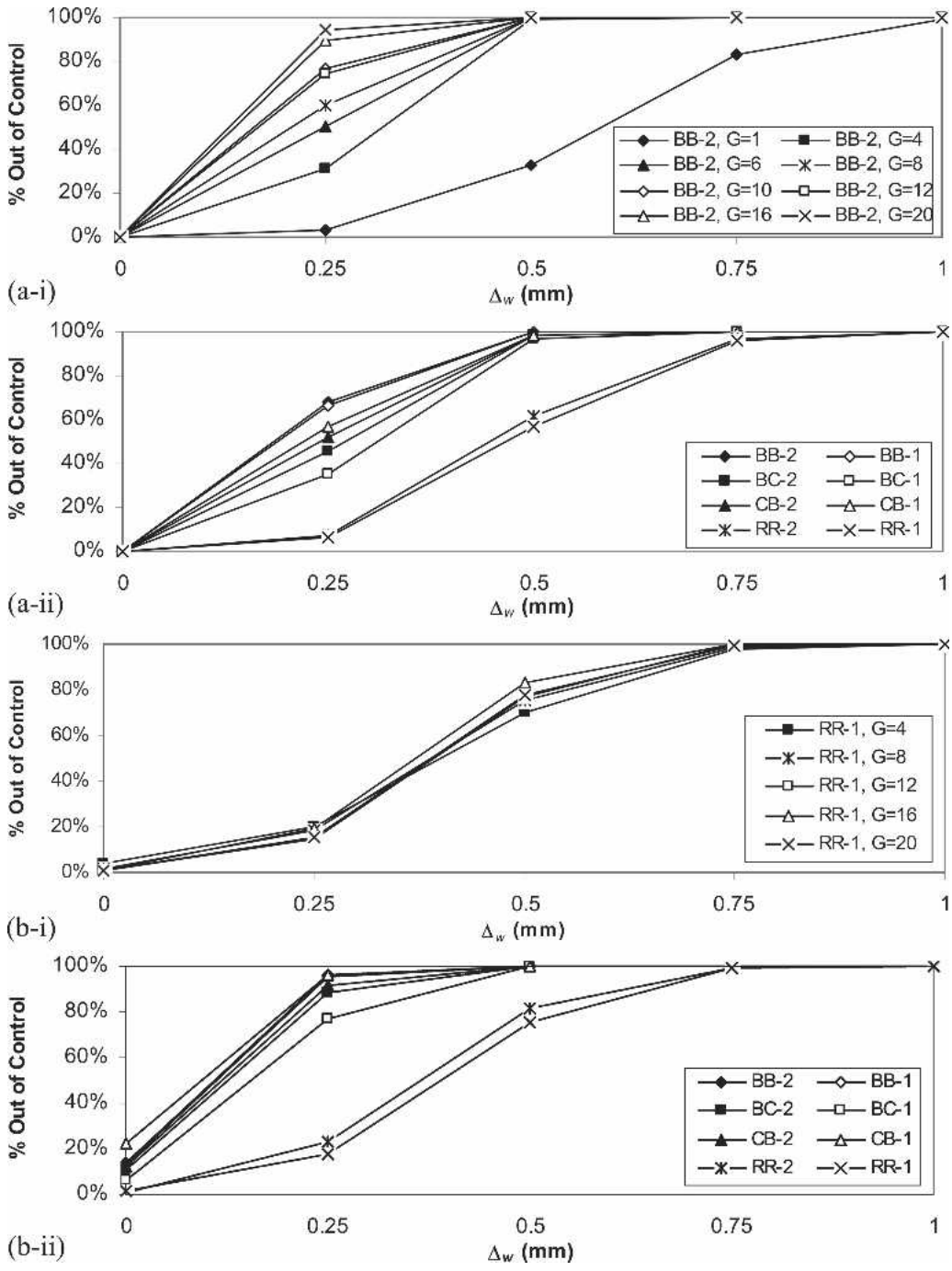

FIG. 7. Percent out-of-control by size of simulated wedge deviation (Δ_w) for (a) $R_{\lambda_{ind}}$ (G = 1) and $R_{\lambda_{grp}}$ charts by: (i) subgroup size (G) for Saw Configuration BB-Side 2, (ii) saw configuration and side (average of all subgroups is shown), (b) S_λ chart by: (i) subgroup size (G) for Saw Configuration RR-Side 1, (ii) saw configuration and side (average of all subgroups is shown).

$R_{\beta\lambda_{grp}}$ charts; because machine positioning deviations were introduced uniformly to each board and laser position, the differences between laser positions by board remained the same. In addition, the introduction of machine positioning deviations did not affect the performance of any of the charts proposed for wedge. Therefore, out-of-control results are not shown for these charts.

DISCUSSION

Five charts were evaluated for their adequacy in detecting machine positioning problems. The $X\text{-bar}_{ind}$ and $X\text{-bar}_{grp}$ charts based on individuals and on subgroups, respectively, performed equally well under in-control conditions. However, the out-of-control response to specific defects varied by size of subgroup. The $X\text{-bar}_{grp}$ chart was more likely to signal when larger subgroups were used, but there is a trade-off in the amount of time necessary to accumulate larger subgroups for sampling. Moreover, with larger subgroup sizes, even the smallest shift in machine positioning ($\Delta_m = 0.25$ mm) caused the charts to signal over 50% of the time. Given normal mill operating conditions, charts constructed with large subgroups may be too sensitive. On the other hand, this sensitivity may be advantageous, as Δ_m must be sustained throughout the subgroup to achieve the reported results.

Although the MR_β and $R_{\beta_{grp}}$ charts performed well during in-control conditions, a shift in machine positioning was indicated by a single out-of-control signal only, and this signal was only noted if the change occurred mid-subgroup. This is in line with findings from Woodall et al. (2000), who, in synthesizing the work of several authors (Rigdon et al. 1994; Sullivan and Woodall 1996), reported that the standard moving range chart (which is applied to the same data as the X-bar chart) is not effective in detecting sustained changes in a process. In this type of situation, a CUSUM chart may be more appropriate.

The S_β chart for between-board variation had similar issues for out-of-control conditions. Moreover, its in-control performance was poor and appeared to be affected by subgroup size. This result was not unexpected, given that the Satterthwaite procedure works well only when $MS_{\beta_{ij}}/MS_{\beta\lambda_{ij}} > F_{(G\text{-}1,G\text{-}1;0.9985)} * F_{(G\text{-}1,G\text{-}1;0.5)}$ (Gaylor and Hopper 1969). This condition is only met for large values of G, and with only a few types of saw configurations (e.g., CB-side 1). A similar result was reported by Maness et al. (2004) in simulation studies using between-board variation values in the same range. This indicates that the S_β chart is inappropriate for the variance components found in typical mill data.

Six charts were evaluated for detecting wedge. The S_λ chart met Gaylor and Hopper's (1969) condition only when monitoring charts for saw configuration RR with larger values of G. On the other hand, the $S_{\beta\lambda}$ chart performed more to expectation, on average, as it met the conditions for every saw configuration and subgroup size. The $S_{\beta\lambda}$ chart, however, did not respond well for out-of-control conditions, remaining virtually unchanged with the addition of wedge defects.

Under out-of-control conditions, the $MR_{\beta\lambda}$ and $R_{\beta\lambda_{grp}}$ charts did not signal. On the other hand, the $R_{\lambda_{ind}}$ and $R_{\lambda_{grp}}$ charts signaled only when Δ_w was >0.5 mm. This response is reasonable, given the range of normal mill conditions. On the other hand, the rate at which out-of-controls were signaled while the process was in control was slightly lower than expected for these charts, which may be caused by non-normality in the profile data (Burr 1967). Since a slight departure from normality appears to be a characteristic of these data, adjustments to chart limits to account for non-normality should be made if these charts are used operationally.

Under ideal conditions, these methods would have been evaluated in the field under operational mill conditions. Thus, a conservative interpretation of these results as tied to this particular LRS arrangement gives only a "proof of concept" verification of the methods. On the other hand, the statistical results are applicable in a wide sense to SPC data arising from multiple sources of variation. Therefore, these results can be interpreted as verifying statistical methods that can be applied to a large variety of real-time manufacturing processes.

There are two main purposes of any SPC system: (1) to provide a signal when defective prod-

ucts are being produced and (2) to identify when processes are performing above expectations (Maness 1993). The SPC systems discussed in this paper go far toward serving these purposes. However, judging if a process is "in-control" must be a decision tailored to the real-time process it is applied to. In the Shewhart sense, a process is in-control when it is not economical to look for assignable causes (Tukey 1946, as cited in Nelson 1999). The implicit assumption in the research relating to this SPC system is that run times associated with 3-sigma limits are long enough for commercial mills. Not only is the occurrence of false alarms costly, but it also leads to a distrust of the SPC system. Using 3-sigma limits may give an average run length (ARL) that is too short for many mills. Consider the pilot set-up at Canfor's Upper Fraser Mill (Upper Fraser, British Columbia, Canada). Typically, six logs are processed per minute at the quad-bandsaw. Assuming a Type I error rate of 0.27%, the ARL is $1/0.0027 \approx 370$, which roughly translates to one false alarm every hour. However, there are multiple control charts being monitored, each with roughly the same possibility of a false alarm. Assuming that the charts are independent (which may be a poor assumption), using two charts increases the Type I error rate to 0.5%, which reduces the ARL by one half, or about 30 minutes of processing.

On the other hand, if the process is truly out-of-control, then out-of-control behavior of the charts should be sustained. Mill personnel should consider whether the process is totally out-of-control and should be stopped, or that the problem is sporadic and should be investigated further. The charts work very well if put in this context. This illustrates the need for mill staff to carefully consider the derivation of their control limits. All the charts that have been introduced in this research could be adjusted to target any ARL. The choice of an ARL will depend on balancing the costs of unnecessary shut down and the costs of producing faulty product.

CONCLUSIONS AND RECOMMENDATIONS

Of the five charts presented for detecting machine positioning problems, the best-performing charts were the X-bar charts, using limits based on the components of variance of the statistical model. The X-bar$_{ind}$ chart provided adequate in-control performance, and was not overly sensitive to minor changes in machine positioning deviations. Therefore, it is recommended for use in real-time SPC.

Of the six charts presented for detecting wedge, the range charts for laser position averages ($R_{\lambda_{ind}}$ and $R_{\lambda_{grp}}$) are recommended, as their out-of-control performance was not overly sensitive and they gave consistent out-of-control rates over all subgroup sizes. However, these charts tended to signal at a rate slightly lower than the expected 0.2% rate, which was likely due to non-normality in the data. Further study should be made to quantify this difference and adjust the values of $D_{0.001}$ and $D_{0.999}$ that are used with this chart accordingly.

Other sawing defects, such as snake, taper, and snipe also occur frequently in production mills; however, summary board data cannot be used to identify them. Instead, alternative control charting techniques need to be considered to best identify their unique qualities. These include techniques for identifying specific trends and monitoring the within-LRS variation (Staudhammer 2004). Research on identifying these kinds of defects is important to fully take advantage of the power of real-time data.

Further testing using truly random samples and field studies would also greatly strengthen the results given here. While simulations provide a verification of the statistical methods presented, mill studies could illuminate the more practical hurdles in making these charts part of a working system for a sawmill SPC system.

The use of real-time LRS data is a reality for many mills today and will likely be more common in the near future. Systems developers must update statistical algorithms to take into account the vastly different data acquired by these devices. Moreover, systems should be designed with non-traditional control charts to take advantage of the opportunity for better sawing defect recognition. Recognition of sawing defects will relate out-of-control signals to specific causes

and help mills to more efficiently find the source of quality problems.

ACKNOWLEDGMENTS

Funding for this project was provided by the National Science and Engineering Research Council of Canada (NSERC), Izaak Walton Killam Foundation, and the British Columbia Science Council. The authors would like to thank Drs. Valerie LeMay, Gary Schajer, and Harry Joe (University of British Columbia) and Mr. Darrell Wong (Forintek Vancouver, Canada) for their contributions to this research, as well as two anonymous reviewers for their helpful comments.

REFERENCES

BURR, I. W. 1967. The effect of non-normality on constants for X-bar and R charts. Industrial Quality Control 24:563–569.

COOK, D. 1992. Statistical process control for continuous forest producers manufacturing operations. Forest Prod. J. 42(7/8):47–53.

DOES, R. J. M. M., K. C. B. ROES, AND A. TRIP. 1999. Handling multivariate problems with univariate control charts. J. Chemometrics 13:353–369.

GAYLOR, D. W., AND F. N. HOPPER. 1969. Estimating the degrees of freedom for linear combinations of mean squares by Satterthwaite's formula. Technometrics 11(4):691–706.

GILBERT, K. C., K. KIRBY, AND C. R. HILD. 1997. Charting autocorrelated data: guidelines for practitioners. Quality Eng. 9(3):367–382.

GRIMSHAW, S. D., AND F. B. ALT. 1997. Control charts for quantile function values. J. Quality Technol. 29(1):1–7.

HARTER, H. L. 1960. Tables of range and studentized range. Ann. Math. Statist. 31(4):1122–1147.

LU, C., AND M. R. REYNOLDS. 1999. Control charts for monitoring the mean and variance of autocorrelated processes. J. Quality Technol. 31(3):259–274.

MANESS, T. C. 1993. Real-time quality control system for automated lumbermills. Forest Prod. J. 43(7/8):17–22.

———, R. A. KOZAK, AND C. L. STAUDHAMMER. 2003. Applying real-time statistical process control to manufacturing processes exhibiting between and within part size variability in the wood products industry. Quality Eng. 16(1):113–125.

———, ———, AND ———. 2004. Reliability testing of statistical process control procedures for manufacturing with multiple sources of variation. Wood Fiber Sci. 36(3):443–458.

MASTRANGELO, C. M., J. M. PORTER, AND R. V. BAXLEY. 2001. Multivariate process monitoring for nylon fiber production. Pages 223–246 *in* Frontiers in Statistical Quality Control. T. Wilrich, ed. Springer-Verlag, New York, NY.

MONTGOMERY, D. C. 2001. Introduction to Statistical Quality Control. John Wiley & Sons, New York, NY.

———, AND C. M. MASTRANGELO. 1991. Some statistical process control methods for autocorrelated data. J. Quality Technol. 23:179–193.

NELSON, L. S. 1999. Notes on the Shewhart control chart. J. Quality Technol. 31(1):124–126.

NOFFSINGER, J. R., AND R. B. ANDERSON. 2002. Effect of autocorrelation on composite panel production monitoring and control: a comparison of SPC techniques. Forest Prod. J. 52(3):60–67.

PADGETT, W. J., AND J. D. SPURRIER. 1990. Shewhart-type charts for percentiles of strength distributions. J. Quality Technol. 22(4):283–290.

PARDO-IGUZQUIZA, E., AND P. A. DOWD. 2004. Normality tests for spatially correlated data. Math. Geol. 36(6):659–681.

RASMUSSEN, H. K., R. A. KOZAK, AND T. C. MANESS. 2004. An analysis of machine caused lumber shape defects in British Columbia sawmills. Forest Prod. J. 54(6):47–56.

RIGDON, S. E., E. N. CRUTHIS, AND C. W. CHAMP. 1994. Design strategies for individuals and moving range control charts. J. Quality Technol. 26(4):274–287.

SAS INSTITUTE. 2002. SAS/STAT User's Guide, Version 8. 8.2, SAS Publishing, Cary, NC.

SHEWHART, W. A. 1931. Economic control of quality of manufactured product. Van Nostrand, New York, NY.

STAUDHAMMER, C. L. 2004. Statistical procedures for development of real-time statistical process control (SPC) systems in lumber manufacturing. Ph.D. Thesis, Department of Wood Science, University of British Columbia, Vancouver, BC, Canada.

———, V. LEMAY, T. C. MANESS, AND R. A. KOZAK. 2005. Mixed-model development of real-time statistical process control data in wood products Manufacturing. Forest Biometry, Modelling, and Information Sciences 1:19–35.

SULLIVAN, J. H., AND W. H. WOODALL. 1996. A control chart for the preliminary analysis of individual observations. J. Quality Technol. 28(3):265–278.

WHEELER, D. J. 1995. Advanced topics in statistical process control. SPC Press, Knoxville, TN.

WOODALL, W. H., R. W. HOERL, A. C. PALM, AND D. J. WHEELER. 2000. Controversies and contradictions in statistical process control. J. Quality Technol. 32(4):341–350.

YOUNG, T. M., AND P. M. WINISTORFER. 1999. SPC. Forest Prod. J. 49(3):10–17.

———, AND ———. 2001. The effects of autocorrelation on real-time statistical process control with solutions for forest products manufacturers. Forest Prod. J. 51(11/12):70–77.

———, ———, AND S. WANG. 1999. Multivariate control charts of MDF and OSB vertical density profile attributes. Forest Prod. J. 49(5):79–86.